Nano Energy 75 (2020) 104951

Contents lists available at ScienceDirect

Nano Energy

journal homepage: http://www.elsevier.com/locate/nanoen

Optogenetic brain neuromodulation by stray magnetic field *via* flash-enhanced magneto-mechano-triboelectric nanogenerator

Han Eol Lee [a,1], Jung Hwan Park [b,1], Dahee Jang [c,1], Jung Ho Shin [d], Tae Hong Im [d], Jae Hee Lee [d], Seong Kwang Hong [d], Hee Seung Wang [d], Min Sub Kwak [e], Mahesh Peddigari [e], Chang Kyu Jeong [f], Yuho Min [e], Chan Hee Park [e], Jong-Jin Choi [e], Jungho Ryu [g], Woon-Ha Yoon [e], Daesoo Kim [c,**], Keon Jae Lee [d,***], Geon-Tae Hwang [e,*]

[a] Department of Mechanical Engineering, Massachusetts Institute of Technology, Cambridge, MA, USA
[b] Department of Mechanical Design Engineering, Kumoh National Institute of Technology, 61 Daehak-ro, Gumi, Gyeongbuk, 39177, Republic of Korea
[c] Department of Biological Sciences, Korea Advanced Institute of Science and Technology (KAIST), 291 Daehak-ro, Yuseong-gu, Daejeon, 34141, Republic of Korea
[d] Department of Materials Science and Engineering, Korea Advanced Institute of Science and Technology (KAIST), 291 Daehak-ro, Yuseong-gu, Daejeon, 34141, Republic of Korea
[e] Functional Ceramics Group, Korea Institute of Materials Science (KIMS), 797 Changwondaero, Seongsan-gu, Changwon, Gyeongnam, 51508, Republic of Korea
[f] Division of Advanced Materials Engineering, Jeonbuk National University, Jeonju, Jeonbuk, 54896, Republic of Korea
[g] School of Materials Science & Engineering, Yeungnam University, Gyeongsan, Gyeongbuk, 38541, Republic of Korea

ARTICLE INFO

Keywords:
Energy harvester
Flash annealing
Magneto-mechano-triboelectric nanogenerator
Flexible micro LED
Optogenetics

ABSTRACT

Optogenetic neuromodulation is a promising technology for continuously caring various neurological diseases. Optogenetic modulating systems were demonstrated by several researchers, but still have critical issues of short lifetime of conventional or biocompatible batteries. Here, we present an optogenetic stimulating system by scavenging wasted magnetic field of home appliance. A flash-enhanced magneto-mechano-triboelectric nanogenerator (MMTENG) was fabricated to demonstrate optogenetic neuromodulation by operating a flexible micro-light-emitting diode (f-μLED). The output performance of MMTENG was enhanced by the flash-induced nano/microscale surface structure of the triboelectric Nylon film. The flash-stamped MMTENG effectively generated an open-circuit peak-to-peak voltage (V_{pp}) of 870 V and a short-circuit current of 145 μA under a gentle alternating current (AC) magnetic field of 7 Oe. A maximum peak power of 8.1 mW was observed from the flash-induced harvester, which was 2.6 times higher than the non-treated device. A high-performance f-μLED with low-resistive ohmic contacts had the improvement of thermal/mechanical stability as well as power efficiency. The MMTENG generated a rectified output voltage of 134 V by a 60 Hz stray magnetic field of home appliance, enabling to operate the f-μLED continuously. An optogenetic stimulator composed of MMTENG and f-μLED was implanted under a living mouse skull without mechanical damage.

1. Introduction

Optogenetics have been recently spotlighted as a strong candidate for advanced neuromodulation technique due to its less tissue damage, high reliability, fast neural response, and cellular-level controllability [1–4]. The genetically-encoded cells rapidly and selectively respond to a light, enabling to remedy various neurological diseases such as epileptic seizure, somnipathy, and Parkinsonism [5–8]. For the optogenetic applications, flexible microscale light-emitting diode (f-μLED) with high power efficiency, low-heating, and thermal/humid/chemical stability could be an excellent light stimulation tool for freely moving animals by achieving conformal attachment on the brain cortex surface with minimal invasion [9–12]. The optogenetic stimulation was demonstrated as a form of implantable electronic system that contains independent

* Corresponding author.
** Corresponding author.
*** Corresponding author.
E-mail addresses: daesoo@kaist.ac.kr (D. Kim), keonlee@kaist.ac.kr (K.J. Lee), gthwang@kims.re.kr (G.-T. Hwang).
[1] These authors contributed equally to this work.

https://doi.org/10.1016/j.nanoen.2020.104951
Received 26 March 2020; Received in revised form 27 April 2020; Accepted 9 May 2020
Available online 30 May 2020

power source of conventional battery [13–15]. However, the restricted lifetime (estimated to ~5 year) of battery could lead to repeated replacements of the discharged battery every several years, which is a medically critical issue especially at an *in-vivo* state [16,17].

Energy harvesting technology based on stray magnetic field is a promising candidate for energy-scavenging biomedical systems since we are ubiquitously surrounded by alternating current (AC) magnetic noise fields [generally less than 1 mT (= 10 Oe) at a fixed frequency of 50/60 Hz] arising from electrical power cables that are installed everywhere including houses, hospitals, factories, and infrastructures [18]. Recently a high-performance magneto-mechano-triboelectric nanogenerator (MMTENG) was reported for demonstration of self-powered internet of things (IoTs) [19]. The MMTENG has been fabricated by employing a magnet-attached cantilever structure and triboelectric materials to initially transduce an AC magnetic field into mechanical oscillations by magnetic force, which is subsequently converted to electricity by the triboelectric effect [19]. With advent of magneto-mechano-triboelectric conversion, lighting up a biomedical f-μLED under an ambient magnetic field could be beneficial to realize battery-free phototherapeutic devices [16,20–23].

Meanwhile, the triboelectrification is represented as a charge transfer process between two different materials of contrary tribopolarities by contact electrification and it has been succesfully introduced into triboelectric nanogenerators (TENGs) for various applications [24–30]. For the performance enhancement of the TENGs, the modification of surface morphology into nano-or micro-scale is a dominant approach since the surface area of the active material strongly influences the friction electrification and contact-induced charges [31,32]. In this regard, light–material interaction (LMI) technologies can be a powerful solution for tuning the surface structure of plastics *via* their exclusive capability to excite multi-scale, transient, localized, and nonequilibrium photon reactions [33–35]. The significant LMI features can photothermally modify the morphology, surface texture, and structural pattern of heat-sensitive polymers [36–46]. Laser sources have been extensively employed to enable immediate tuning of the surface morphology of plastic films *via* accurate controllability of processing parameters for sophisticated heat transfer including energy density, wavelength, and pulse duration [47]. Although pulsed lasers can sharply raise and lower the temperature of polymers within an extremely confined focal area to facilitate local ablation, patterning, or shaping of their topmost layer, they have a severe limitation in achieving mass productivity due to the serial processing flow [48]. From the viewpoints of a scalable and cost-effective light source, Xenon flash lamps have attracted extensive attention owing to their instantaneous and large-area process-ability, high light producing efficiency, and excellent compatibility with mass production as roll-to-roll process [37,38,49–52].

Herein, we developed a flash-enhanced MMTENG with multi-dimensional triboelectric surface morphology for the demonstration of optogenetic brain neuromodulation by operating an *in-vivo* vertical-structured f-μLED. Light absorbing copper oxide nanoparticles (CuO NPs) were intermediately introduced on a triboelectric Nylon film as a heating amplifier and a plastic stamping template upon flash lamp processing. By irradiating a millisecond flash light, nanoscale bumpy texture and a microscale wrinkle structure were simultaneously formed on a Nylon surface *via* multiscale interface interactions between CuO NPs and the polymer substrate, which significantly increased the active friction area. A cantilever-structured MMTENG was fabricated with a flash-stamped Nylon film and a normal Teflon sheet as triboelectric counterpart materials. The flash-enhanced MMTENG generated an open-circuit peak-to-peak voltage (V_{pp}; the distance from the highest positive amplitude to the lowest negative amplitude in the voltage graph) of 870 V and a short-circuit current of 145 μA under a gentle AC magnetic field of 7 Oe at 133 Hz arising from a Helmholtz coil. The harvester also shows a maximum peak power of 8.1 mW, which was 2.6 times higher compared to the non-patterned device. For optogenetic manipulation by scavenging the wasted energy in home appliance, a high-performance red f-μLED was realized by low-resistive ohmic contacts and vertical interconnections of electrodes. The f-μLED exhibited excellent thermal/mechanical/chemical stability under a high irradiating power density of 10 mW/mm^2. The MMTENG was located near a 60 Hz magnetic noise field of a common home appliance to generate an open-circuit rectified voltage of 134 V, which was large enough to turn on the f-μLED. Finally, the optogenetic f-μLED array was smoothly slid through a small cranial slit (2.5 × 4 mm^2) of a mouse with conformal covering on the curved and corrugated brain surface. The behavioral transitions successfully occurred by illuminating red LED light pulses on the mouse motor cortex.

2. Experimental section

2.1. Characterization of multiscale morphology nylon film

The morphologies and texture of the flash-stamped Nylon film was characterized by SEM (S-4800, Hitachi), and AFM (XE-100, Park Systems). The chemical and elemental compositions of the Nylon substrate treated by flash stamping process was monitored with XPS (Sigma Probe, Thermo VG Scientific) in an area of 1.5 cm × 1.5 cm.

2.2. Finite element method simulation

Flash-inducted heating simulation was implemented by COMSOL Multiphysics 5.3 software. The simulation model was constructed to similar structure with actual experiments (4 layers of CuO NPs on a nylon substrate). The thermal conductivity, capacity and density of each materials in the calculations are as in the following: k_{CuO}: 32.9 W/m·K, $C_{p,\ CuO}$: 550.5 J/kg·K, ρ_{CuO}: 6310 kg/m^3, k_{Nylon}: 0.26 W/m·K, C_{Nylon}: 1700 J/kg·K, and ρ_{Nylon}: 1150 kg/m^3. The irradiation condition of the flash light was pulse width of 3 ms, and energy density of 20 J/cm^2.

2.3. Measurement of the output performance of the MMTENG

The output voltage of MMTENG was characterized by a digital oscilloscope (WaveSurfer 44Mx-A, Teledyne Lecroy) and the current signal of MMTENG was measured by a multi-sourcemeter (Keithley 2611A).

2.4. Fatigue test of flash-enhanced MMTENG

The fatigue test of flash-enhanced MMTENG was conducted inside the Helmholtz coil with inducing AC magnetic field of 7 Oe at 133 Hz. The open-circuit output voltage of MMTENG was recorded by the oscilloscope during whole 10^6 vibration cycles.

2.5. Metallic ohmic contacts between p-AlGaInP and metal layers

Transmission line method was used to accurately measure the contact resistance between p-AlGaInP and metal layers [53]. The contact resistance was computed by the following equation.

$$WR_T = R_sL+2WR_c$$

where W, R_T, R_s, L, and R_c is the line width, the total resistance, the sheet resistance, line gap, and the contact resistance, respectively. Following contact metals were applied in the measurements: Au (100 nm), Ni/Ge/Au (10/10/100 nm), Ti/Au (10/100 nm) and Cr/Au (10/100 nm) layers. All metal layers were patterned with width of 100 μm, and length of 10, 20, 40, 80 and 160 μm. The contact resistivity was redefined by the following equation.

$$\rho_c = R_cLW$$

where ρ_c is the contact resistivity between p-AlGaInP and contact metal

layers.

2.6. Animals

Animal care and experiments were conducted according to the guidelines of the Animal Care and Use Committee of the Korea Advanced Institute of Science and Technology (KAIST) and were approved by the Institutional Animal Care and Use Committee (Protocol No. KA2014-05). Male C57BL/6J mice, aged 7–8 weeks, were maintained under a 12-h light/dark cycle with ad libitum access to food and water.

2.7. Stereotactic virus injection and histology

Mice were anesthetized with 2,2,2-tribromoethanol (Avertin 2.5%) via intraperitoneal injection and placed on a motorized stereotaxic frame (Neurostar, Gemany). For photostimulation of motor neurons, the motor cortex (AP, +1.5mm; ML, −1.5mm; DV, -1mm, from bregma) was injected with AAV8-Syn-ChrimsonR-tdTomato (University of North Carolina Vector Core, USA) at a rate of 0.05 μl/min using a 33-gauge blunt needle (World Precision Instruments, USA). A total 3.0 μl of virus mixture was injected at a titer of 5×10^{12} genome copies [gc]/ml

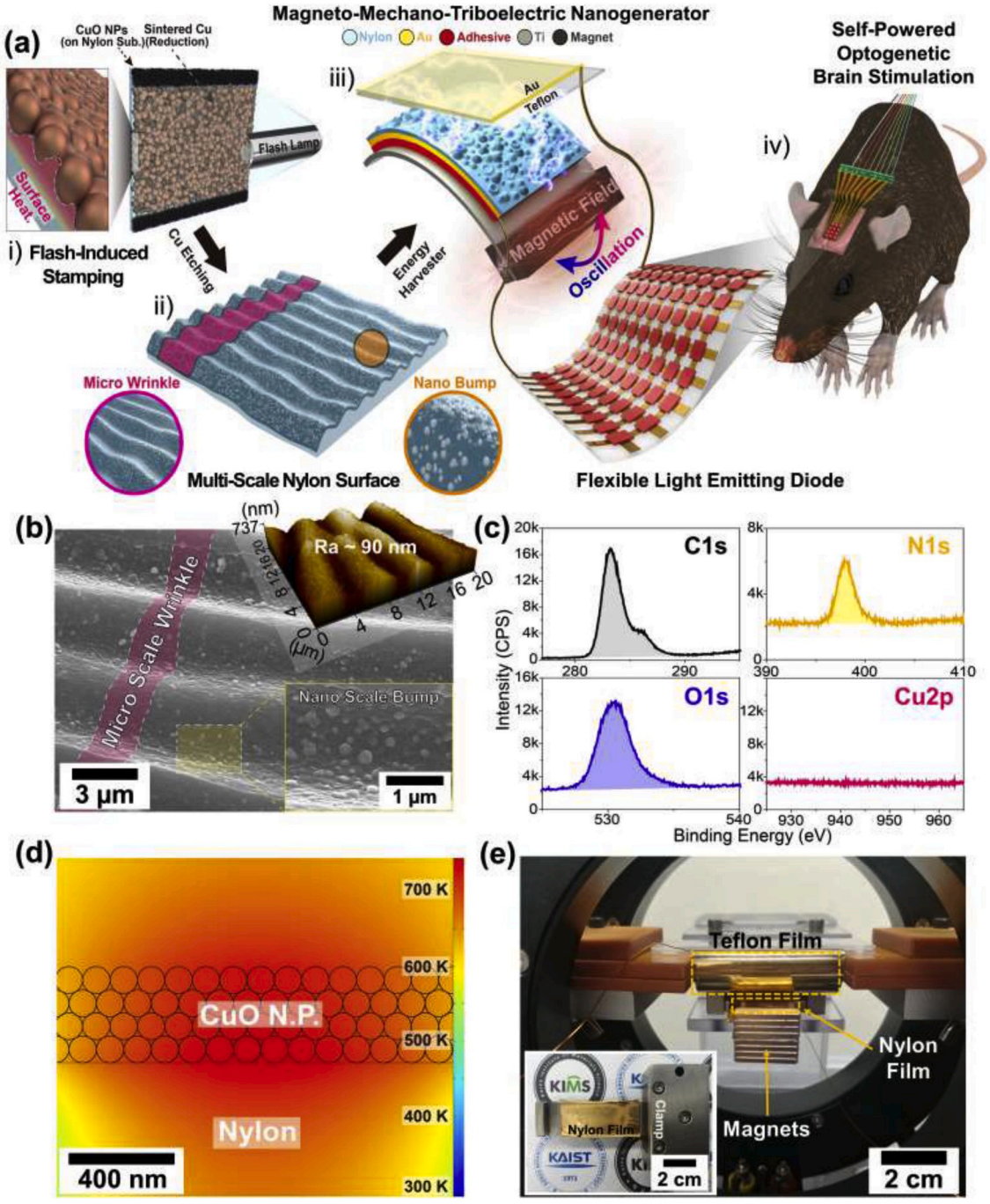

Fig. 1. (a) Schematic illustration of the fabrication process for flash-induced MMTENG and its application for optogenetics by energy-scavenging. (b) Plane-view SEM image of the flash-stamped multiscale Nylon film. Top right inset illustrates the AFM image of the Nylon substrate processed by flash stamping procedure. The bottom right inset shows the magnified SEM image of the nanoscale bump structure of the flash-treated Nylon surface. (c) XPS results of the flash-induced Nylon sheet after Cu etching process. (d) FEA simulation result that presents the CuO/Nylon temperature generated by flash light irradiation (energy density of 20 J/cm^2, pulse width of 3 ms). (e) Photograph of the MMTENG inside the Helmholtz coil. The inset presents the cantilever structure with flash-induced Nylon film.

into the left motor cortex. For microscopic imaging of viral expression and brain structure, mice were anesthetized with an intraperitoneal Avertin (2.5%) injection and transcardially perfused with PBS followed by 4% formaldehyde solution. Their brains were extracted and incubated in 4% formaldehyde solution for an additional 12 h after perfusion. After fixation, the brain samples were sectioned (40 μm thickness) on a vibratome. Brain imaging was performed on a confocal microscope (A1 HD25 Confocal Microscope, KAIST Bio Core Center).

2.8. Optogenetic stimulation of the motor cortex

Cranial windows (2.5 × 4 mm^2) were made on the left hemisphere, 1.0 mm posterior from bregma, 3 weeks after viral injections. The optogenetic f-μLED was implanted beneath the skull by sliding the device through the cranial window to contact the cortical surface. To monitor whisker movements, imagery analysis system was utilized while the motor cortical areas were stimulated by the f-μLED array. To measure the movement of the whiskers, video recordings were analyzed using ImageJ software (MTrack2 plugin).

3. Result and discussion

Fig. 1a schematically illustrates the device fabrication process of the flash-enhanced MMTENG and its application to turn on the vertical-structured f-μLED. The following is a detailed explanation: i) CuO nano ink (Novacentrix, ICI–002HV) as an intermediate heating amplifier and a polymer-imprinting layer was spin-coated onto a Nylon film (thickness of 50 μm). The light absorptive CuO NPs (band gap of 1.2 eV, particle diameter of ~100 nm) effectively converted the photon energy of a broad flash spectrum from 200 nm to 1μm into thermal energy, which caused a drastic photothermal interaction at the Cu (photo-reduced) and plastic interface that created a rough polymer surface. ii) The morphology of the Nylon substrate emerged after etching the flash-induced Cu layer, showing greatly increased surface area by the microscale wrinkle structure and nanoscale bumpy texture. iii) To fabricate a cantilever-type flash-enhanced MMTENG (see Fig. S1 in the Supporting Information), the backside of the flash-stamped Nylon film was sputtered with the Au electrode, and adhered on a Ti plate (thickness of 300 μm) by adhesive. Next, several NdFeB magnets were fixed at the end of the Ti cantilever structure as tip masses, facilitating induction of repeated up and down second harmonic resonant vibrations of the cantilever under an AC magnetic field. The Au coated Teflon sheet (thickness of 100 μm) was placed on the overhead area of the Nylon surface as a negative triboelectric part. The combination of Nylon and Teflon layers enabled high performance triboelectric power generation owing to their positive and negative charge affinities. As a result, the MMTENG could convert the ambient AC magnetic field to electric energy to turn on the optogenetic f-μLED. iv) The high performance f-μLEDs were implanted between the mouse skull and brain. The MMTENG-connected f-μLEDs radiated the pulsed red light to the primary and secondary motor cortices for artificial behavior controls.

Fig. 1b presents a scanning electron microscope (SEM) image of the Nylon surface demonstrated by the flash stamping process. The flash light with a pulse width of 3 ms and an energy density of 20 J/cm^2 was irradiated to the introduced light absorbing CuO layer to generate intense photothermal energy, which was indirectly transferred into the CuO NP/polymer interface. The rapid interfacial heat with optimized flash-power successfully induced localized tuning of the Nylon surface rather than causing global polymer damage. After the flash lamp processing, a Cu etching procedure was performed to completely remove the photo-reduced Cu template and sequentially expose the polymer surfaces (Figs. 1b and S2). A microscale wrinkled structure could be formed on a Nylon surface by flash-induced heating and quenching interaction occurred at the interface between the polymer and CuO NPs. As a first stage, the flash-induced photothermal energy was diffused into the Nylon, extending the polymer surface by thermal expansion. After the irradiation of a single pulsed millisecond flash, the expanded Nylon was subsequently cooled down and contracted, producing compressive strain at the polymer interface. This flash-induced uniform stress caused the bucking of the Nylon surface, creating a regularly wrinkled structure on the polymer film [36]. As shown in the right top inset of Fig. 1b, the wavelength and the amplitude of the polymer wrinkles were measured as 5 μm and 200 nm, respectively, by an atomic force microscope (AFM). Simultaneously, flash-activated instant melting and solidifying reaction of the Nylon surface created interfacial interlocking structure based on the convoluted CuO stamp framework, resulting in polymer film with nanoscale bump morphology (right bottom inset of Fig. 1b). Our flash lamp system equipped with a parabolic reflector evenly distributed the flash light intensity onto the CuO-coated Nylon sample, leading to a homogeneous heating over a large area without generating significant thermal gradient. This uniform heat energy identically induced photothermal interaction (e.g., microscale wrinkling and nanoscale interlocking) at the CuO and Nylon interface, which enabled the nylon with evenly rough surface throughout the entire light irradiated region. The demonstrated multidimensional texture of the polymer top layer presented huge surface area, exhibiting ~31 times higher average roughness (R_a: 90 nm) than the pristine Nylon sheet (R_a: 2.849 nm) in Fig. S3 (see the Supporting Information). Note that the nano-and micro--polymer structure *via* the flash-induced stamping process could significantly increase triboelectric contact area and frictional force, which enabled abundant surface charges compared to the flat plastic substrate [31]. We believe that the surface area and resulting triboelectric properties of the flash-enhanced multiscale Nylon surface can be further improved by optimizing the various processing factors, including modulus of the applied materials, film thickness, and photothermal temperature. Fig. S4 in the Supporting Information presents a top SEM image of the polymer film treated by flash light in the absence of CuO nanomaterial. Since most of the photon energy was not absorbed by the CuO NPs but instead transmitted through the transparent plastic substrate, the morphology of the Nylon surface could not be changed *via* flash lamp processing. Fig. 1c shows X-ray photoelectron spectroscopy (XPS) data of the flash-stamped Nylon sheet to confirm the clean polymer surface. Normal XPS peaks of Nylon, including C1s, N1s, and O1s, were distinctly observed, whereas the Cu2p peak was not identified. Therefore, we could conclude that the Cu etching procedure thoroughly eliminated the flash-induced Cu residue, which may deteriorate the performance of the triboelectric energy harvester due to its negative charge affinity. In addition, the XPS data of the flash-induced Nylon exhibited similar peak intensity and position compared to that of the pristine Nylon film (Fig. S5), which showed that the chemical composition of the both Nylon sheets are nearly identical. We believe that the ultrafast flash-induced heating and cooling effect successfully induced photothermal imprinting process without altering the chemical structure of the Nylon.

Due to the difficulties of direct measurement of the surface temperature of the Nylon film during flash light processing, a finite element analysis (FEA) simulation was carried out to verify the surface modification capability of the polymer substrate via intensive photothermal interaction between flash light and CuO NPs/Nylon, as described in Fig. 1d. The temperature of the CuO NPs and plastic film after the flash light irradiation process was calculated by the heat flux equation (1) [54]:

$$Q = \rho C \frac{\partial T}{\partial t} + \rho C \cdot \nabla T - \nabla \cdot (k \nabla T) \quad (1)$$

Here, Q is the thermal energy induced by the flash light annealing and C, ρ, and k are the heat capacity, density, and thermal conductivity of the CuO NPs and Nylon, respectively (detailed information is provided in the experimental section). Intense photon energy absorbed by CuO nanomaterials could be efficiently converted to thermal energy and subsequently transferred to the Nylon sheet, increasing the temperature of the polymer surface up to 750 K in 3 ms. This instantaneous heating

and cooling interaction at the CuO/polymer interface could sufficiently cause surface texturing of the Nylon with a low melting temperature of 250 °C.

Fig. 1e presents the experimental measurement setup for the flash-enhanced MMTENG under the AC magnetic field arising from the Helmholtz coil. The clamped cantilever structure composed of a flash-stamped Nylon sheet, Ti substrate, and permanent magnets is shown in the inset of Fig. 1e. The Teflon film was placed above the vibrating cantilever body with the optimizing gap distance about 1 mm to acquire maximum output (see Fig. S6 in the Supporting Information) [19]. The Helmholtz coil facilitated the generation of an AC magnetic field around the cantilever beam, and the amount of magnetic field was adjusted by modulation of the input AC current on the coil. The attached magnets on the MMTENG enabled continuous up and down bending resonant oscillations of the cantilever by interactive attraction and repulsion with the surrounding magnetic field. The detailed working mechanism for the MMTENG under the second harmonic bending resonance mode is provided in Figs. S7 and S8 (see the Supporting Information). To check the effect of flash structures on Nylon film on the triboelectric potential, we carried out an analytical simulation compared to the normal flat Nylon surface, which is presented in Fig. S9 (see the Supporting Information).

We measured the electric output signals of the MMTENG in the

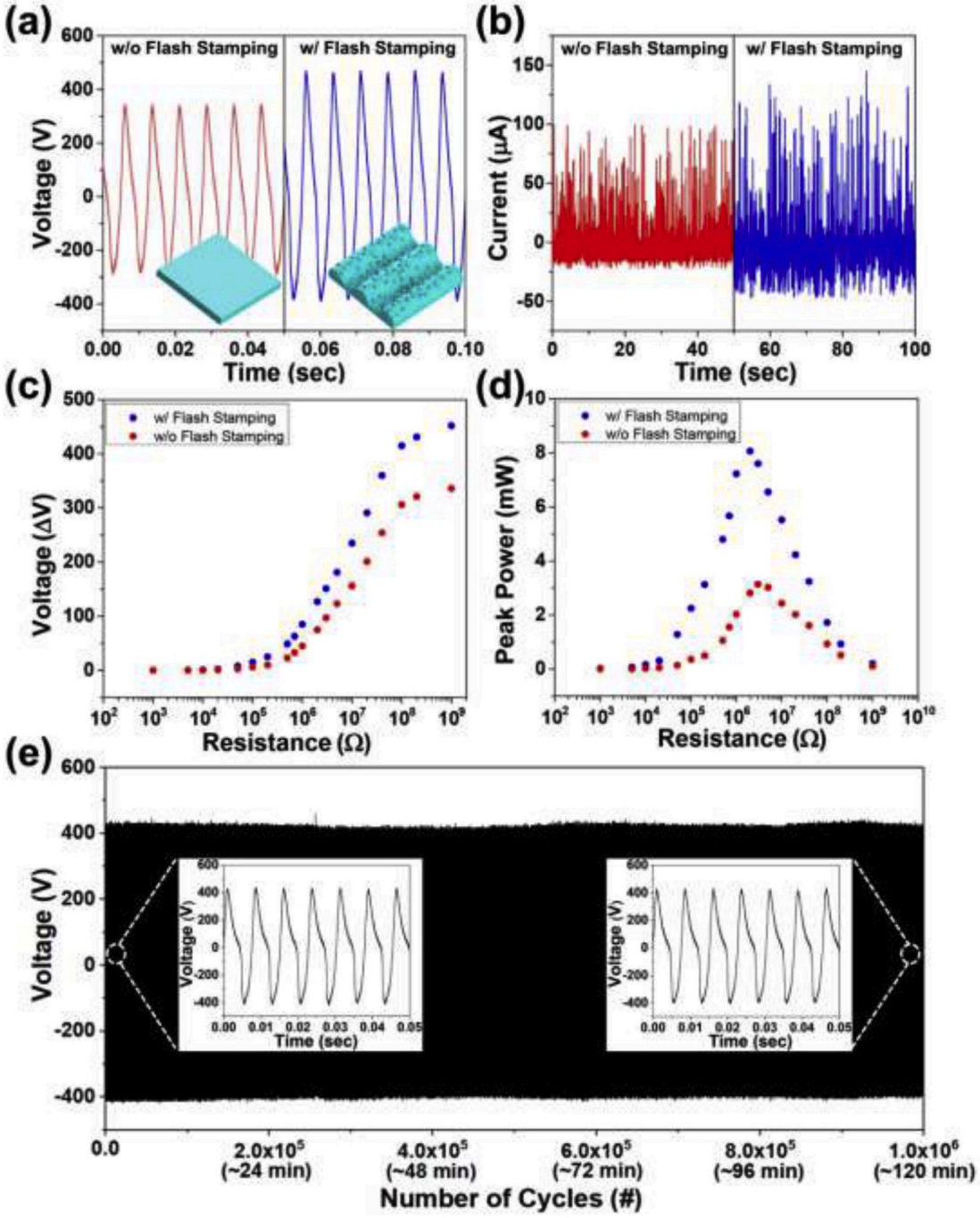

Fig. 2. (a) The open-circuit voltage signals without and with flash-enhanced MMTENG. (b) The short-circuit current signals without and with flash stamping MMTENG. (c) The absolute peak voltages with various external resistances between 1 kΩ and 1 GΩ from the MMTENG without and with flash stamping. (d) The peak powers according to dependence of load resistance for MMTENG without and with flash stamping. (e) The harvesting stability test of flash-enhanced MMTENG during 1 million (over 2 h) vibration cycles.

Helmholtz coil. The whole area of the cantilever structure was 60 × 20 mm^2, and the area of the attached Nylon sheet for triboelectric energy harvesting was 50 × 20 mm^2. The second harmonic resonance frequency of the MMTENG device was about 133 Hz by attaching eight permanent magnets (a total weight of 12 g) at the end of the cantilever structure. The vibration displacements of cantilever structure as a dependence of the magnet numbers are presented in Fig. S10 (see the Supporting Information). To confirm the effect of flash-induced multiscale stamping on the Nylon surface for the triboelectric harvesting performance, the output signals of flash-enhanced and pristine (flat nylon; control) samples were compared at a same AC magnetic field of 7 Oe. For the Nylon film with the nano-and micro-morphology, the MMTENG generated an open-circuit V_{pp} of 870 V (see Video S1) and a short-circuit current up to 145 μA, whereas the control sample generated only an open-circuit V_{pp} of 638 V and a short-circuit current of 100 μA, as presented in Fig. 2a and b.

Supplementary video related to this article can be found at https://doi.org/10.1016/j.nanoen.2020.104951

The output current signal shows relatively large fluctuation compared to the voltage output since the sourcemeter system does not offer high-resolution time-domain measurement of current output. It would randomly measure the current signal of MMTENG, thus deriving non-stable output current value. The open-circuit output voltage was increased with the improvement of the magnetic field and nearly saturated from the point of 7 Oe since the increment of the output was noticeably decreased between 7 Oe and 11 Oe compared to the region of 3 Oe to 7 Oe (Fig. S11 in the Supporting Information). Note that the vibration displacement of cantilever structure was gradually increased with enhancement of AC magnetic field. For the triboelectric contact and separation mode, the output voltage is related to the amount of transferred charges ($\triangle\sigma$) between opposite two electrodes of counterpart triboelectric materials. The $\triangle\sigma$ is directly determined by the separation distance of the two triboelectric plates. When the separation distance starts to increase from a contact state, the $\triangle\sigma$ is rapidly increased, and then the slope of $\triangle\sigma$ curve starts to decrease until reaching at a saturation point (; the slope of $\triangle\sigma$ becomes nearly zero). By this reason, the open-circuit output voltage of contact and separation TENG could be saturated above an optimum separation distance between two triboelectric materials [55]. The flash lamp annealing process for the multi-scale triboelectric polymer surface derived noticeable enhancement of the output voltage and current signals, by 36% and 45%, respectively, during the harvesting operation. To verify the peak output power between flash-stamped and non-stamped MMTENG devices, the peak voltage ($\triangle V$; the maximum voltage value at the AC voltage signal) was measured with external load resistances ranging from 1 kΩ to 1 GΩ under an AC magnetic field of 7 Oe at 133 Hz as shown in Fig. 2c and d (corresponding output current signals are presented in Fig. S12 of the Supporting Information). The $\triangle V$ signals gradually built up as the resistance increased and became saturated at a high load resistance. To calculate the peak power of the MMTENG, we divided the value of $\triangle V^2$ into the external resistance ($P = \triangle V^2/R$, where P is the peak power and R is the resistance). From the result, a maximum peak power of 8.1 mW at a resistance of 2 MΩ was obtained from the surface modified device, which was 2.6 times higher compared to the control sample with the maximum peak power of 3.1 mW at a resistance of 3 MΩ. Since the power of MMTENG is proportional to the square of voltage value at a resistance, the flash process has derived noticeable enhancement of output power, which would be beneficial to demonstrate broad application field [19]. This is enabled by effective friction between two counterpart materials and larger contact area, thus resulting in more surface charges compared to the flat polymer film [31]. The optimum external resistance to derive maximum output power of contact-mode triboelectric nanogenerator is reversely proportional to the surface area of triboelectric material. The equation for optimum resistance (R_{opt}) is given by $R_{opt} = (d_o + x_{max})^2/S{\cdot}v{\cdot}\varepsilon_0$, where d_0 is the effective thickness constant (given by $d_o = d_1/\varepsilon_1 + d_2/\varepsilon_2$, where d_1 and ε_1 are the thickness and relative dielectric constant of triboelectric material #1, d_2 and ε_2 are the thickness and relative dielectric constant of triboelectric material #2), x_{max} is the optimum separation distance between two triboelectric materials, S is the area size of triboelectric materials, v is the constant velocity during contact-mode, and ε_0 is the permittivity of free space [56]. Future integration of electromagnetic generator or piezoelectric nanogenerator into MMTENG to suggest new hybrid-type magneto-electric (ME) generator would be required to improve the performance of ME harvester to demonstrate various self-powered applications [27,57–63].

A fatigue test was also conducted to survey the output stability and mechanical durability of the flash-enhanced MMTENG. As shown Fig. 2e, the output voltage signals were consistently recorded without notable degradation during 1 million cycles (over 2 h). The insets of Fig. 2e present the time-dependent open-circuit V_{pp} values at the initial stage (866 V) and 1 million cycles (850 V). The outstanding durability of the MMTENG was attributed to the robust wear resistance properties of the Nylon and Teflon films under the significant repeated frictions. In addition, our MMTENG device could generate considerable power through the mild contact between the freestanding Teflon and gently oscillating Nylon that attached on a thin (300 μm in thickness) Ti cantilever. Thus, the significantly reduced physical force was applied between the triboelectric layers during the repeated mechanical loading, resulting in high durability of the MMTENG. To experimentally confirm the robustness of our MMTENG device, we observed the morphologies of the nano/microscale Nylon film after long-term fatigue test by SEM characterization. As shown in the SEM images in Fig. S13, the flash-induced multiscale surface structures exhibited no severe abrasion in spite of the 1 million vibration cycles. Meanwhile, the conventional wireless energy transmission system (e.g., inductive power transfer) in biomedical devices may produce excessive heating inside the body, thus severely threatening the safety of biological tissue [64]. To confirm the thermal stability of our device, the temperature of the triboelectric Nylon surface (before and after durability test) was checked by an infrared thermal imaging camera as shown in Fig. S14 (see the Supporting Information). From the images, notable thermal change was not found through the mechanical durability test, which could be an advantage for demonstrating a sustainable energy-scavenging biomedical system [65].

Fig. 3a shows an optical image of the vertical-structured f-μLED array in the bent state (bending curvature radius of 2 cm). To fabricate the f-μLED brain stimulator, AlGaInP-based LED layers were deposited by metalorganic chemical vapor deposition on a mother GaAs substrate. After metal thin-film deposition and an annealing process, low-resistive ohmic contacts were made on the p-AlGaInP layer. The μLED chips were formed by Ar/Cl_2 gas-based dry etching, and isolated by an ultraviolet (UV)-cured polymer layer. After p-electrode deposition on μLED chips, a biocompatible polymer was covered to protect the device from mechanical and chemical damages. The rigid GaAs wafer was selectively eliminated by wet-etchant for device flexibility, and then metallic n-electrodes were formed on the flipped device for vertical interconnection (see Fig. S15 in the Supporting Information for the detailed procedure). As shown in the lower inset of Fig. 3a, the fabricated f-μLED had a sharp peak wavelength of 650 nm, which was a suitable wavelength for stimulating a red-shifted channelrhodopsin (chrimson, CnChR1) for the optogenetic stimulation [9,66].

Enhancement of power efficiency is the most important factor of the μLED for the effective neural stimulation during biomedical applications. The μLED efficiency is closely related with the contact resistivity between semiconductor and metal layers. In order to reduce the contact resistivity of the μLED array, metallic ohmic contacts were optimized by adjusting the annealing temperature and contact materials [67–69]. Fig. 3b presents the contact resistivity between LED layers and four different contact metals (Au, Ni/Ge/Au, Ti/Au, and Cr/Au) as a function of annealing temperature. A minimum contact resistivity among several conditions was 4.18 × 10^{-6} Ω cm^2 from 300 °C-annealed Cr/Au layers

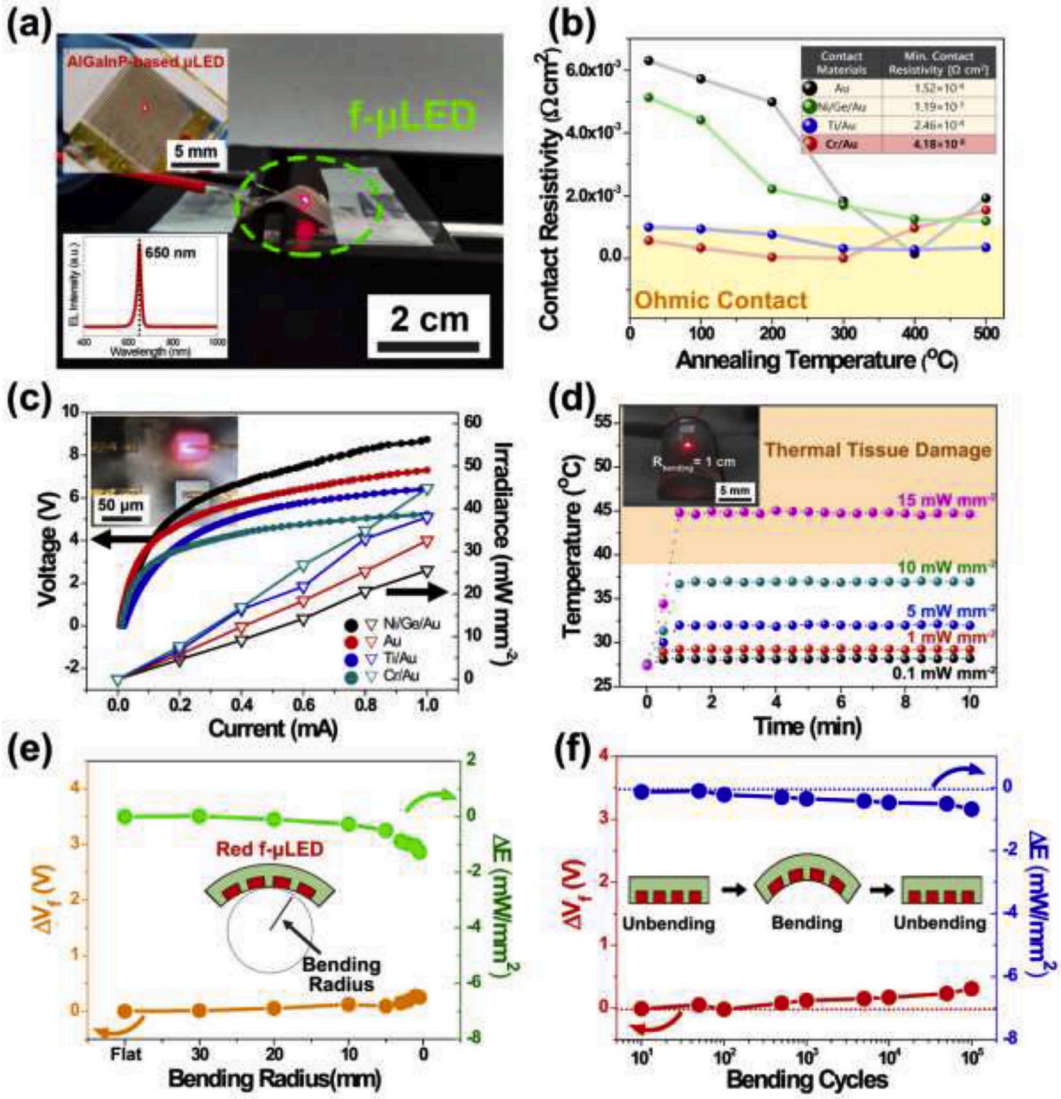

Fig. 3. (a) A photograph of the vertical-structured f-μLED under a bending condition. The upper inset is a top view of AlGaInP-based flexible red μLED. The lower inset is electroluminescence spectra of the red μLED. (b) Contact resistivity graphs between LED layer and four different metal layers. (c) Luminance-current-voltage (L-I-V) graphs of f-μLED with various metal contacts. The inset is a magnified image of a 50 x 50 μm^2-sized red LED chip. (d) LED temperature during constant light emission (bending curvature radius of 1 cm). (e) Electrical/optical characteristics of red f-μLED under nine different bending radiuses. (f) Results of reliability test during 100,000 periodic bending motions. (For interpretation of the references to color in this figure legend, the reader is referred to the Web version of this article.)

on a p-AlGaInP, which was 50 times lower than that of the Ti/Au contacts. As the heating temperature increased, the contact resistivity of μLED gradually decreased regardless of the contact materials. Above the specific annealing temperature, however, the contact resistivity built up due to the exfoliation of metal layers, as shown in Fig. S16 (see the Supporting Information). Optimization effects of the metallic ohmic contacts are revealed in the luminance-current-voltage (L-I-V) graph of Fig. 3c. The inset of Fig. 3c exhibits a magnified optical image of 50 x 50 μm^2-sized f-μLED with metallic contacts. The turn-on voltage of the optimized f-μLED was measured to be about 2 V, which was 0.5–2 V lower than other contact materials. Furthermore, the f-μLED with 300 °C-annealed Cr/Au contacts had outstanding irradiance of 44.78 mW/mm^2 at injection current of 1 mA. We chose this 300 °C-annealed Cr/Au ohmic contacts for f-μLED-based photo-stimulator, due to its high optical power and low energy consumption.

The thermal stability of f-μLED is a significant issue for wearable and optogenetic devices for *in-vivo* brain photostimulation without thermal tissue damages. To verify the thermal advantage of the optimized f-μLED, the device temperature was experimentally measured for 10 min. Fig. 3d shows the temperature changes of f-μLED at five different light irradiance conditions (0.1, 1, 5, 10, and 15 mW/mm^2). The temperatures of the f-μLED proportionally increased as time passed, and were finally saturated at 44, 36, 31, 29, and 28 °C for 15, 10, 5, 1, and 0.1 mW/mm^2, respectively. The inset of Fig. 4d displays the bent f-μLED with illuminating power density of 10 mW/mm^2 on a half-cylindrical polymer mold. The temperature of the f-μLED was stably maintained under 37 °C during light emission of the irradiance from 1 to 10 mW/mm^2, which is the threshold energy for optogenetic activation [70,71]. According to these results, the red f-μLED was suitable to activate the chrimson-expressed neurons on optogenetics without thermal tissue damage because the device temperature did not exceed the mammalian body temperature [72,73]. Chemical strength is an important factor of the f-μLED for *in-vivo* optogenetic stimulation. To verify that, soaking test was fulfilled in 1x phosphate-buffered saline (PBS) solution. As shown in Fig. S17 (see the Supporting Information), the f-μLED in PBS exhibited negligible irradiance decrease of ~0.2 mW/mm^2 for 26 h. Mechanical flexibility of the f-μLED is essential for application of the brain-attached photostimulation due to the curved and corrugated

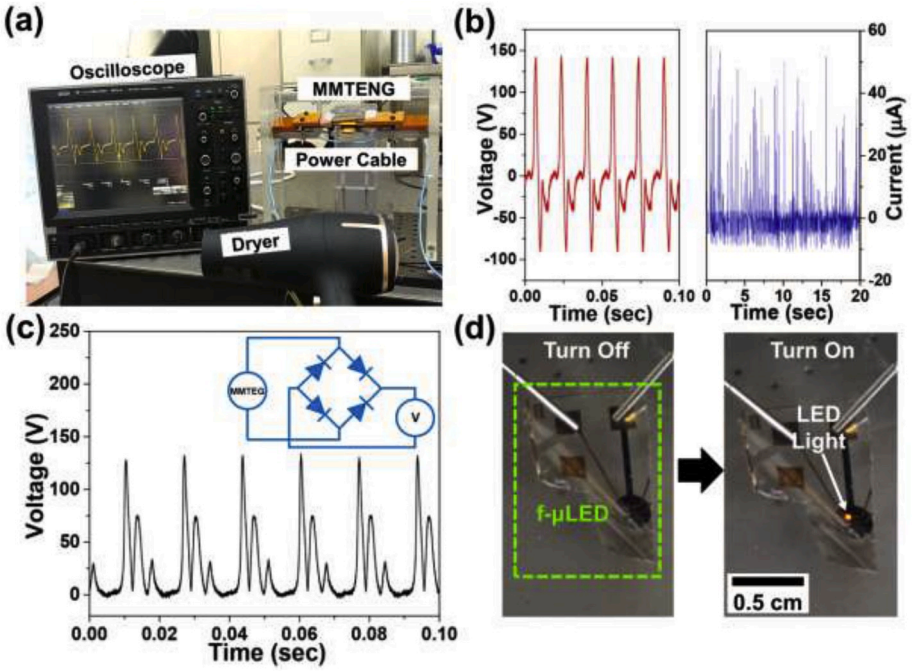

Fig. 4. (a) A photograph of the MMTENG near an electric wire linked to a dryer. (b) Open-circuit voltage and short-circuit current values from the MMTENG near a stray magnetic field. (c) Rectified output voltage measured from the MMTENG near the power cable. The inset shows a circuit diagram of the rectifying process. (d) A photograph of the f-μLED lighted up by the rectified signal of the MMTENG.

structure of the mammalian brain. Bending stability tests were carried out at different bending radii (1, 2, 3, 4, 5, 10, 20, and 30 mm), as shown in Fig. 3e. In spite of the bending radius decrement, the red f-μLED presented negligible degradations in their irradiance (1.27 mW/mm^2) and forward voltage (0.25 V). Fig. 3f displays the fatigue test results of f-μLED at a bending radius of 2 mm. After severe bending/unbending motions of 100,000 cycles, the forward voltage increased by 6.67% (0.31 V), and the optical power density decreased by 4.53% (0.68 mW/mm^2).

Powering of the f-μLED was investigated using the MMTENG under a stray 60 Hz AC magnetic field generated from an electric power cable of a household appliance. Fig. 4a shows the experimental setup consisting of the MMTENG, an electric wire connected to a hairdryer, and an oscilloscope. For this experiment, we utilized a Ti cantilever (size of 65 x 20 × 0.2 mm^2), a flash-enhanced Nylon film (size of 50 × 20 mm^2), and eight mass magnets (a total weight of 12 g) to tune the resonance frequency of the MMTENG to 60 Hz. The electric wire was located under the magnets of the cantilever structure with a distance about 1mm to arouse a strong magnetic response between the tip mass magnets and the magnetic field. By turning on the hairdryer, root mean square (RMS) current of 9.5 A was flowed through the electric cable as shown in Fig. S18 (see the Supporting Information). The induced AC magnetic field at the end of triboelectric cantilever may be 2.1 Oe, which was calculated by Ampère's law on the electric wire ($B = \mu_0 \cdot I/2 \cdot \pi \cdot r$, where B: magnetic field, μ_0: permeability of free space, I: flowing current on the power cable, r: radius or distance from the center of power cable). The MMTENG device generated a 60 Hz open-circuit V_{pp} of 237 V and a short-circuit current of 33 μA, as presented in Fig. 4b (see Video S2). During the vibration, the magnets made repeated gentle touching with electric wire (see Fig. S19 in the Supporting Information), which could generate secondary vibration, thus causing additional regular peaks following the normal voltage signals. For successful lighting of the f-μLED, the AC-type output signal of MMTENG should be converted into the direct current (DC) value using a full bridge-rectifying circuit. Fig. 4c shows the output voltage (maximum value of 134 V) of the MMTENG connected to a commercial rectifier, and the inset presents the circuit diagram of the rectifying process. The f-μLED device was continuously operated on using the rectified 60 Hz electric output of the MMTENG under the stray AC magnetic field (see Video S3), as shown in Fig. 4d. During the energy harvesting of MMTENG, the maximum input voltage and current signals for f-μLED were 9.5 V and 41.8 μA, respectively as shown in Fig. S20 (see the Supporting Information). From this result, we estimate that the peak input power of 0.4 mW (from the equation of P═VI, where P is the power, V is the voltage, and I is the current) was supplied into f-μLED from the MMTENG. By using a suitable degree of a power generated by MMTENG, f-μLED emitted a light with irradiance of ~2.14 mW/mm^2. The red light with ~2.14 mW/mm^2 is sufficient power for activating light sensitive protein [74,75].

Supplementary video related to this article can be found at https://doi.org/10.1016/j.nanoen.2020.104951

The magnetic field is proportionally decreased with the increment of distance from the current flowing cable, thus the output performance of MMTENG is severely influenced by distance of electric wire. However, if we introduce a very big Helmholtz coil at a room as a biomedical application in the future, this problem could be simply solved. The Helmholtz coils can make uniform and stable magnetic field inside the active area, thus able to minimize the spatial restriction of MMTENG. Moreover, the guideline of limiting exposure for magnetic field [established by the International Commission on Non-Ionizing Radiation Protection (ICNIRP)], recommends 2 Oe (at 60 Hz) for general public places and 10 Oe (at 60 Hz) for occupational places [76]. Based on these facts, we performed a new experiment to turn on the f-μLED using MMTENG located at different (bottom and upper) regions inside the Helmholtz coil with inducing AC magnetic field of 2 Oe as shown in Fig. S21 (see the Supporting Information). With these operations of MMTENG, the f-μLED was sucessfully lit up by electric energy generated from the tiny 2 Oe of magnetic field, which was a good example against the spatial restriction of MMTENG in the application field. To confirm the working stability of f-μLED, the MMTENG supplied the electric energy into f-μLED for 20 h under AC magnetic field of 2 Oe induced by the Helmholtz coil (for long-term operation), and the f-μLED succesfully irradiated the red light during 20 h (see Fig. S22 in the Supporting Information). In general, the μLEDs with a pulse operation have 2–4 times longer lifetime than a constant operation due to its small heat

accumulation in the device. Based on our experimental results of a constant (Fig. S17 in the Supporting Information) and pulse operation (Fig. S22 in the Supporting Information), it is estimated that our f-μLED can be used to optogenetic brain stimulation for minimum several days by using MMTENG as the pulsed-power source [77,78]. This estimated usage time is enough to realize brain stimulation, considering that researchers irradiated light to brain for several minutes to hours in the recent papers [79–81]. This energy-scavenging demonstration verified that the MMTENG could constantly supply electric energy to the f-μLED without a battery or an external power source. Although the MMTENG can light up the f-μLED with a simple diode bridge to rectify the AC signal into DC signal in this work, a high conversion efficiency circuit for TENG is strongly required to effectively operate other internet of thing (IoT) devices and charge secondary batteries, which could increase applicability and universality of MMTENG technology [82].

To directly test whether the MMTENG is sufficient to stably provide electricity to the vertical-structured f-μLED *in-vivo*, a brain stimulation with a pulsed light (pulse duration of ~10 ms) was demonstrated to activate cortical neurons of living mouse [83]. Before the experiment, AAV-Syn-ChrimsonR-tdTomato was injected into the mouse brain as an AAV viral vector, which harbored Chrimson into the frontal motor cortical area. As a red light-activated channelrhodopsin variant, Chrimson was expressed in the primary motor cortex (M1). When the red light from the f-μLED is irradiated into the Chrimson-modified neural cells of M1, permeation of cations across the cell membrane occurred, thus enabling neural excitation to deliver a motor command to the brainstem circuitry for whisker retraction [84–88]. Fig. 5a shows an experimental illustration of the energy-scavenging optogenetic modulation using a living mouse, f-μLED array operated by the MMTENG, and a simplified neural pathway corresponding to the whisker movement. Fig. 5b presents an image of an anesthetized mouse located on a stereotaxic fixture with the *in-vivo* f-μLED to stimulate the M1. The f-μLED device was inserted over the mouse brain surface under the skull in a less invasive manner as shown in Fig. S23 (see the Supporting information). And, the f-μLEDs were exactly located on the specific region of M1 surface which is a whisker movement-related area, as a previous work [9].

To trigger whisker movement of the mouse, the f-μLED was powered by the MMTENG (the same device as shown in Fig. 4, operated by the noise magnetic field) with induction of a tiny AC magnetic field of 2.1 Oe at 60 Hz (see experiment setup in Fig. S24 of the Supporting Information). As a result, the energy-scavenging optogenetic system could produce red LED light with ~10 ms duration by the rectified MMTENG output signal. During the optogenetic stimulation, the vibration of the whisker was tracked utilizing video capture and image analysis as shown in Fig. 5c–i (see Video S4). Fig. 5c–ii presents the whisker movement triggered *via* the optogenetic procedure for 2 s (120 frames), and the tip position of the whisker was changed with a noticeable alternation during the recoding frames of a 1/60 s interval, which is obviously compared to the control test (see Fig. S25 in the Supporting Information). This result indicates that our MMTENG device under a gentle magnetic field could be used as an efficient energy-scavenging deivce for the optogenetic f-μLED to define the functions of mammalian cortical areas.

After the optogenetic neuromodulation on the mouse brain, a post-mortem histological analysis was performed to verify the expression of Chrimson in the M1 region. With settlement of Chrimson into the M1 neurons, the movement of mouse whisker utilizing the *in-vivo* f-μLED could be practical evidence of successful optogenetic manipulation [66, 84–89]. The top of Fig. 5d shows a confocal fluorescent image of the cortex to investigate the Chrimson injection site, and an intensive fluorescent red color signal (normally generated by tdTomato; a maker of Chrimson) is observed at the stimulation site of M1. Since the auto-fluorescence backgrounds (fixative-generated fluorescence and fluorescence of inherent tissue elements) of tdTomato overlapped on both the neural cells and brain tissue, the nuclei of the M1 neurons were dyed using 4′ 6-diamidino-2-phenylindole (DAPI) to confirm whether the Chrimson was expressed from neuronal cells [90,91]. If the Chrimson (red signal) and DAPI (blue signal) appeared at the same points, it means that these locations are Chrimson-modified neurons. The bottom images of Fig. 5d show magnified views of the stimulated M1 region. Even though the Chrimson and DAPI signals were widely distributed in the observed area, several red/blue superimposed signals (pointed by white arrows) were discovered on the 'Merged' image, thus demonstrating the successful optogenetic stimulation with the f-μLED array. In addition, identical brain morphology (see Fig. S26 in the Supporting information) confirmed that minimal damage occurred in the frontal motor cortex after f-μLED implantation through DAPI staining.

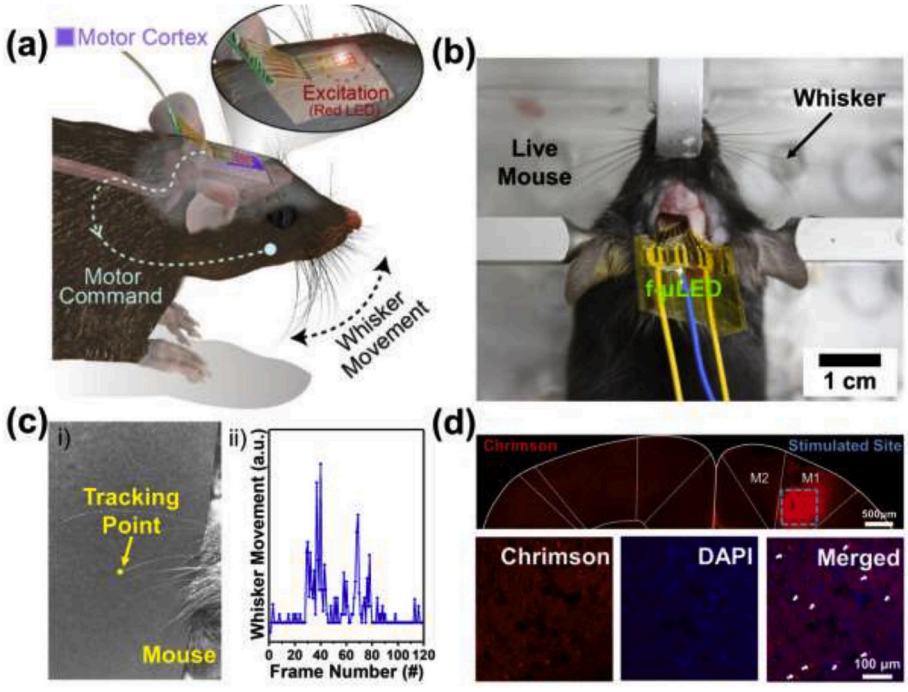

Fig. 5. (a) Schematic depiction of experimental procedures for energy-scavenging optogenetic brain stimulation. (b) Implantation of f-μLED array underneath the mouse skull for stimulation of M1. (c) i) Video tracking of the whisker movements. The yellow circle is the tracking point. ii) Relative whisker movements *via* f-μLED stimulation with MMTENG operation. (d) Confocal fluorescent images of mouse brain. The top is the expression of Chrimson and the stimulation site in the motor cortex. The bottom is a magnified image for the stimulated M1 site. Red color signals indicate the expression of tdTomato (a maker of Chrimson), and the blue signals represent the DAPI (a maker of neural cells). (For interpretation of the references to color in this figure legend, the reader is referred to the Web version of this article.)

Supplementary video related to this article can be found at https://doi.org/10.1016/j.nanoen.2020.104951

4. Conclusion

In summary, we report a flash-stamped MMTENG operated under a gentle AC magnetic field to induce an optogenetic behavioral change of a live animal. The flash light with a pulse width of 3 ms and an energy density of 20 J/cm^2 successfully demonstrated a multiscale (micro-wrinkle and nano-bump) Nylon structure *via* photothermal interactions at the CuO NPs/polymer interface, significantly increasing the triboelectric surface roughness by ~310%. We believe that this flash-induced surface texturing method can be extensively applied to provide simple ways for demonstrating numerous multidimensional polymer surface structure for high-performance TENG device. With an AC magnetic field of 7 Oe, the MMTENG generated open-circuit V_{pp} and short-circuit current signals of 870 V and 145 μA, respectively. A maximum peak power of 8.1 mW was obtained from the flash-enhanced MMTENG at an external load resistance of 2 MΩ. This superior output performance of the triboelectric device originated from the multidimensional morphology of the flash-treated Nylon film, which derived improvements of contact tribo-electrification as well as electrostatic induction with noticeable operation durability during 1 million operating cycles. The vertical-structured red f-μLED with low-resistive metal contacts exhibits outstanding electrical efficiency, showing an irradiance of 44.78 mW/mm^2 at 1 mA. The f-μLED temperature was stably maintained under normal body temperature during high-powered irradiation of 10 mW/mm^2. The MMTENG was introduced near a 60 Hz electric wire connected to a dryer to generate an open-circuit V_{pp} and a short-circuit current of 237 V and 33 μA, respectively, and then the signal was rectified to light the f-μLED. Finally, our energy-scavenging optogenetic stimulator was smoothly inserted under the mouse skull to radiate red light into the intended brain region. We verified that the whisker movements of a living mouse were caused by the precise Chrimson activation in the light-emitted motor cortex. These results indicate that the energy-scavenging brain photostimulator is powerful tool for investigating the neuro-muscular interactions and the ethological modulations of mammalians. The continuous optogenetic manipulation by using the wasted magnetic field around us including home, hospital, factory, and infrastructure could be used as a novel therapeutic protocol to derive behavior change or even treat life-threatening neurodiseases. We currently have a future plan to develop a long-term optogenetic stimulation using a small-scale and high-performance MMTENG with a biocompatible passivation, which can be implanted in large mammalians (e.g., canine and porcine) [92–95]. This procedure would require a complete packaging technique such as conventional non-magnetic titanium case or biocompatible polymer coating for MMTENG to prevent permeation of body fluid into triboelectric friction surface since the moisture on the active area could cause severe harvesting performance degradation by discharging behavior of surface charges [96].

Declaration of competing interest

The authors declare that they have no known competing financial interests or personal relationships that could have appeared to influence the work reported in this paper.

CRediT authorship contribution statement

Han Eol Lee: Writing - original draft. **Jung Hwan Park:** Writing - original draft. **Dahee Jang:** Writing - original draft. **Jung Ho Shin:** Data curation. **Tae Hong Im:** Data curation. **Jae Hee Lee:** Investigation. **Seong Kwang Hong:** Investigation. **Hee Seung Wang:** Methodology. **Min Sub Kwak:** Methodology. **Mahesh Peddigari:** Data curation. **Chang Kyu Jeong:** Formal analysis. **Yuho Min:** Methodology. **Chan Hee Park:** Investigation. **Jong-Jin Choi:** Methodology. **Jungho Ryu:** Formal analysis. **Woon-Ha Yoon:** Investigation. **Daesoo Kim:** Writing - original draft. **Keon Jae Lee:** Writing - original draft. **Geon-Tae Hwang:** Writing - original draft.

Acknowledgements

H. E. Lee, J. H. Park, and D. Jang contributed equally to this work. The work at KIMS was supported by the National Research Council of Science & Technology (NST) grant by the Korea government (MSIP) (No. CAP-17-04-KRISS), NRF grant funded by the Korea government (MSIT) (No. 2019R1C1C1003765). The work at KAIST was supported by Creative Materials Discovery Program (Grant No. NRF-2016M3D1A1900035), Nano Material Technology Development Program (Grant No. NRF-2016M3A7B4905621), Brain Research Program (2017M3C7A1029612 to D. Kim), the Bio & Medical Technology Development Program (2019M3E5D2A01066259 to D. Kim) through the National Research Foundation of Korea (NRF) funded by the Ministry of Science and ICT. This paper is based on a research which has been conducted as part of the KAIST-funded Global Singularity Research Program for 2020. The work at YU was supported by NRF grant funded by the Korea government (MSIT) (No. 2019R1A2B5B01070100). Dr. H. E. Lee was supported by Basic Science Research Program through the National Research Foundation of Korea (NRF) funded by the Ministry of Education (2019R1A6A3A12031643).

Appendix A. Supplementary data

Supplementary data to this article can be found online at https://doi.org/10.1016/j.nanoen.2020.104951.

References

[1] E. Pastrana, Optogenetics: controlling cell function with light, Nat. Methods 8 (2011) 24–25.
[2] K. Deisseroth, Optogenetics, Nat. Methods 8 (2011) 26–29.
[3] C. Wyart, F. Del Bene, E. Warp, E.K. Scott, D. Trauner, H. Baier, E.Y. Isacoff, Optogenetic dissection of a behavioural module in the vertebrate spinal cord, Nature 461 (2009) 407–410.
[4] A.H. Park, S.H. Lee, C. Lee, J. Kim, H.E. Lee, S.B. Paik, K.J. Lee, D. Kim, Optogenetic mapping of functional connectivity in freely moving mice via insertable wrapping electrode array beneath the skull, ACS Nano 10 (2016) 2791–2802.
[5] J. Tonnesen, A.T. Sorensen, K. Deisseroth, C. Lundberg, M. Kokaia, Optogenetic control of epileptiform activity, Proc. Natl. Acad. Sci. U.S.A. 106 (2009) 12162–12167.
[6] V. Gradinaru, M. Mogri, K.R. Thompson, J.M. Henderson, K. Deisseroth, Optical deconstruction of parkinsonian neural circuitry, Science 324 (2009) 354–359.
[7] A.R. Adamantidis, F. Zhang, A. Aravanis, K. Deisseroth, L. de Lecea, Neural substrates of awakening probed with optogenetic control of hypocretin neurons, Sleep 31 (2008) A364.
[8] A.V. Gourine, V. Kasymov, N. Marina, F.G. Tang, M.F. Figueiredo, S. Lane, A. G. Teschemacher, K.M. Spyer, K. Deisseroth, S. Kasparov, Astrocytes control breathing through pH-dependent release of ATP, Science 329 (2010) 571–575.
[9] S.H. Lee, J. Kim, J.H. Shin, H.E. Lee, I.S. Kang, K. Gwak, D.S. Kim, D. Kim, K.J. Lee, Optogenetic control of body movements via flexible vertical light-emitting diodes on brain surface, Nano Energy 44 (2018) 447–455.
[10] H.E. Lee, J.H. Choi, S.H. Lee, M.J. Jeong, J.H. Shin, D.J. Joe, D.H. Kim, C.W. Kim, J.H. Park, J.H. Lee, D.S. Kim, C.S. Shin, K.J. Lee, Monolithic flexible vertical GaN light-emitting diodes for a transparent wireless brain optical stimulator, Adv. Mater. 30 (2018), 1800649.
[11] H.E. Lee, J.H. Shin, J.H. Park, S.K. Hong, S.H. Park, S.H. Lee, J.H. Lee, I.S. Kang, K. J. Lee, Micro light-emitting diodes for display and flexible biomedical applications, Adv. Funct. Mater. 29 (2019), 1808075.
[12] H.E. Lee, S.H. Lee, M. Jeong, J.H. Shin, Y. Ahn, D. Kim, S.H. Oh, S.H. Yun, K.J. Lee, Trichogenic photostimulation using monolithic flexible vertical AlGaInP light-emitting diodes, ACS Nano 12 (2018) 9587–9595.
[13] J.A. Cardin, M. Carlen, K. Meletis, U. Knoblich, F. Zhang, K. Deisseroth, L.H. Tsai, C.I. Moore, Targeted optogenetic stimulation and recording of neurons *in vivo* using cell-type-specific expression of channelrhodopsin-2, Nat. Protoc. 5 (2010) 247–254.
[14] S.H. Yun, S.J.J. Kwok, Light in diagnosis, therapy and surgery, Nat. Biomed. Eng. 1 (2017) 8.
[15] A.R. Adamantidis, F. Zhang, A.M. Aravanis, K. Deisseroth, L. De Lecea, Neural substrates of awakening probed with optogenetic control of hypocretin neurons, Nature 450 (2007) 420–424.

[16] G.T. Hwang, Y. Kim, J.H. Lee, S. Oh, C.K. Jeong, D.Y. Park, J. Ryu, H. Kwon, S. G. Lee, B. Joung, D. Kim, K.J. Lee, Self-powered deep brain stimulation via a flexible PIMNT energy harvester, Energy Environ. Sci. 8 (2015) 2677–2684.

[17] Y. Zhao, C.B. Liu, Z.X. Liu, W.H. Luo, L.Z. Li, X. Cai, D. Liang, Y.Z. Su, H. Ding, Q. Wang, L. Yin, J.S. Guan, M.M. Luo, X. Sheng, Wirelessly operated, implantable optoelectronic probes for optogenetics in freely moving animals, IEEE Trans. Electron. Dev. 66 (2019) 785–792.

[18] J. Ryu, J.E. Kang, Y. Zhou, S.Y. Choi, W.H. Yoon, D.S. Park, J.J. Choi, B.D. Hahn, C. W. Ahn, J.W. Kim, Y.D. Kim, S. Priya, S.Y. Lee, S. Jeong, D.Y. Jeong, Ubiquitous magneto-mechano-electric generator, Energy Environ. Sci. 8 (2015) 2402–2408.

[19] K.W. Lim, M. Peddigari, C.H. Park, H.Y. Lee, Y. Min, J.W. Kim, C.W. Ahn, J.J. Choi, B.D. Hahn, J.H. Choi, D.S. Park, J.K. Hong, J.T. Yeom, W.H. Yoon, J. Ryu, S.N. Yi, G.T. Hwang, A high output magneto-mechano-triboelectric generator enabled by accelerated water-soluble nano-bullets for powering a wireless indoor positioning system, Energy Environ. Sci. 12 (2019) 666–674.

[20] S.H. Lee, C.K. Jeong, G.T. Hwang, K.J. Lee, Self-powered flexible inorganic electronic system, Nano Energy 14 (2015) 111–125.

[21] D.H. Kim, H.J. Shin, H. Lee, C.K. Jeong, H. Park, G.T. Hwang, H.Y. Lee, D.J. Joe, J. H. Han, S.H. Lee, J. Kim, B. Joung, K.J. Lee, In vivo self-powered wireless transmission using biocompatible flexible energy harvesters, Adv. Funct. Mater. 27 (2017), 1700341.

[22] Q. Zheng, B.J. Shi, Z. Li, Z.L. Wang, Recent progress on piezoelectric and triboelectric energy harvesters in biomedical systems, Adv. Sci. 4 (2017), 1700029.

[23] R. Hinchet, H.-J. Yoon, H. Ryu, M.-K. Kim, E.-K. Choi, D.-S. Kim, S.-W. Kim, Transcutaneous ultrasound energy harvesting using capacitive triboelectric technology, Science 365 (2019) 491–494.

[24] F.R. Fan, Z.Q. Tian, Z.L. Wang, Flexible triboelectric generator, Nano Energy 1 (2012) 328–334.

[25] Z.L. Wang, Triboelectric nanogenerators as new energy technology for self-powered systems and as active mechanical and chemical sensors, ACS Nano 7 (2013) 9533–9557.

[26] W. Seung, M.K. Gupta, K.Y. Lee, K.S. Shin, J.H. Lee, T.Y. Kim, S. Kim, J. Lin, J. H. Kim, S.W. Kim, Nanopatterned textile-based wearable triboelectric nanogenerator, ACS Nano 9 (2015) 3501–3509.

[27] S.H. Wang, X.J. Mu, X. Wang, A.Y. Gu, Z.L. Wang, Y. Yang, Elasto-aerodynamics-driven triboelectric nanogenerator for scavenging air-flow energy, ACS Nano 9 (2015) 9554–9563.

[28] Y. Lee, W. Kim, D. Bhatia, H.J. Hwang, S. Lee, D. Choi, Cam-based sustainable triboelectric nanogenerators with a resolution-free 3D-printed system, Nano Energy 38 (2017) 326–334.

[29] J. Luo, Z. Wang, L. Xu, A.C. Wang, K. Han, T. Jiang, Q. Lai, Y. Bai, W. Tang, F. R. Fan, Z.L. Wang, Flexible and durable wood-based triboelectric nanogenerators for self-powered sensing in athletic big data analytics, Nat. Commun. 10 (2019) 5147.

[30] J. Luo, F.R. Fan, T. Zhou, W. Tang, F. Xue, Z.L. Wang, Ultrasensitive self-powered pressure sensing system, Extrem. Mech. Lett. 2 (2015) 28–36.

[31] C.K. Jeong, K.M. Baek, S.M. Niu, T.W. Nam, Y.H. Hur, D.Y. Park, G.T. Hwang, M. Byun, Z.L. Wang, Y.S. Jung, K.J. Lee, Topographically-designed triboelectric nanogenerator via block copolymer self-assembly, Nano Lett. 14 (2014) 7031–7038.

[32] K.N. Kim, J. Chun, J.W. Kim, K.Y. Lee, J.U. Park, S.W. Kim, Z.L. Wang, J.M. Baik, Highly stretchable 2D fabrics for wearable triboelectric nanogenerator under harsh environments, ACS Nano 9 (2015) 6394–6400.

[33] D.J. Joe, S. Kim, J.H. Park, D.Y. Park, H.E. Lee, T.H. Im, I. Choi, R.S. Ruoff, K. J. Lee, Laser–material interactions for flexible applications, Adv. Mater. 29 (2017), 1606586.

[34] T.F. Hong, W.J. Ju, M.C. Wu, C.H. Tai, C.H. Tsai, L.M. Fu, Rapid prototyping of PMMA microfluidic chips utilizing a CO_2 laser, Microfluid. Nanofluidics 9 (2010) 1125–1133.

[35] F. Liang, J. Lehr, L. Danielczak, R. Leask, A.M. Kietzig, Robust non-wetting PTFE surfaces by femtosecond laser machining, Int. J. Mol. Sci. 15 (2014) 13681–13696.

[36] J.H. Park, J. Seo, C. Kim, D.J. Joe, H.E. Lee, T.H. Im, J.Y. Seok, C.K. Jeong, B.S. Ma, H.K. Park, T.S. Kim, K.J. Lee, Flash-induced stretchable Cu conductor via multiscale-interfacial couplings, Adv. Sci. 5 (2018), 1801146.

[37] J.H. Park, S. Han, D. Kim, B.K. You, D.J. Joe, S. Hong, J. Seo, J. Kwon, C.K. Jeong, H.J. Park, T.S. Kim, S.H. Ko, K.J. Lee, Plasmonic-tuned flash Cu nanowelding with ultrafast photochemical-reducing and interlocking on flexible plastics, Adv. Funct. Mater. 27 (2017), 1701138.

[38] J.H. Park, G.T. Hwang, S. Kim, J. Seo, H.J. Park, K. Yu, T.S. Kim, K.J. Lee, Flash-induced self-limited plasmonic welding of silver nanowire network for transparent flexible energy harvester, Adv. Mater. 29 (2017), 1603473.

[39] J.H. Park, S. Jeong, E.J. Lee, S.S. Lee, J.Y. Seok, M. Yang, Y. Choi, B. Kang, Transversally extended laser plasmonic welding for oxidation-free copper fabrication toward high-fidelity optoelectronics, Chem. Mater. 28 (2016) 4151–4159.

[40] H. Palneedi, J.H. Park, D. Maurya, M. Peddigari, G.T. Hwang, V. Annapureddy, J. W. Kim, J.J. Choi, B.D. Hahn, S. Priya, K.J. Lee, J. Ryu, Laser irradiation of metal oxide films and nanostructures: applications and advances, Adv. Mater. 30 (2018), 1870094.

[41] H.S. Kim, S.R. Dhage, D.E. Shim, H.T. Hahn, Intense pulsed light sintering of copper nanoink for printed electronics, Appl. Phys. A 97 (2009) 791–798.

[42] J.Y. Long, P.X. Fan, D.W. Gong, D.F. Jiang, H.J. Zhang, L. Li, M.L. Zhong, Superhydrophobic surfaces fabricated by femtosecond laser with tunable water adhesion: from lotus leaf to rose petal, ACS Appl. Mater. Interfaces 7 (2015) 9858–9865.

[43] T.H. Her, R.J. Finlay, C. Wu, S. Deliwala, E. Mazur, Microstructuring of silicon with femtosecond laser pulses, Appl. Phys. Lett. 73 (1998) 1673–1675.

[44] H.M. Jin, D.Y. Park, S.J. Jeong, G.Y. Lee, J.Y. Kim, J.H. Mun, S.K. Cha, J. Lim, J. S. Kim, K.H. Kim, K.J. Lee, S.O. Kim, Flash light millisecond self-assembly of high χ block copolymers for wafer-scale sub-10 nm nanopatterning, Adv. Mater. 29 (32) (2017), 1700595, https://doi.org/10.1002/adma.201700595.

[45] C.K. Jeong, S.B. Cho, J.H. Han, D.Y. Park, S. Yang, K.I. Park, J. Ryu, H. Sohn, Y. C. Chung, K.J. Lee, Flexible highly-effective energy harvester via crystallographic and computational control of nanointerfacial morphotropic piezoelectric thin film, Nano Res. 10 (2017) 437–455.

[46] T. Jeon, H.M. Jin, S.H. Lee, J.M. Lee, H.I. Park, M.K. Kim, K.J. Lee, B. Shin, S. O. Kim, Laser crystallization of organic–inorganic hybrid perovskite solar cells, ACS Nano 10 (8) (2016) 7907–7914, https://doi.org/10.1021/acsnano.6b03815.

[47] H. Pazokian, A. Selimis, J. Barzin, S. Jelvani, M. Mollabashi, C. Fotakis, E. Stratakis, Tailoring the wetting properties of polymers from highly hydrophilic to superhydrophobic using UV laser pulses, J. Micromech. Microeng. 22 (2012), 035001.

[48] S. Baudach, J. Bonse, W. Krautek, Ablation experiments on polyimide with femtosecond laser pulses, Appl. Phys. A 69 (1999) S395–S398.

[49] J. Perelaer, R. Abbel, S. Wunscher, R. Jani, T. van Lammeren, U.S. Schubert, Roll-to-roll compatible sintering of inkjet printed features by photonic and microwave exposure: from non-conductive ink to 40% bulk silver conductivity in less than 15 seconds, Adv. Mater. 24 (2012) 2620–2625.

[50] D. Angmo, T.T. Larsen-Olsen, M. Jorgensen, R.R. Sondergaard, F.C. Krebs, Roll-to-roll inkjet printing and photonic sintering of electrodes for ITO free polymer solar cell modules and facile product integration, Adv. Energy Mater. 3 (2013) 172–175.

[51] T.H. Im, D.Y. Park, H.K. Lee, J.H. Park, C.K. Jeong, D.J. Joe, K.J. Lee, Xenon flash lamp-induced ultrafast multilayer graphene growth, Part. Part. Syst. Char. 34 (2017), 1600429.

[52] J.H. Park, H.E. Lee, C.K. Jeong, D.H. Kim, S.K. Hong, K.I. Park, K.J. Lee, Self-powered flexible electronics beyond thermal limits, Nano Energy 56 (2019) 531–546.

[53] S. Eidelloth, R. Brendel, Analytical theory for extracting specific contact resistances of thick samples from the transmission line method, IEEE Electron. Device Lett. 35 (2014) 9–11.

[54] D.H. Jung, J.H. Park, H.E. Lee, J. Byun, T.H. Im, G.Y. Lee, J.Y. Seok, T. Yun, K. J. Lee, S.O. Kim, Flash-induced ultrafast recrystallization of perovskite for flexible light-emitting diodes, Nano Energy 61 (2019) 236–244.

[55] S. Wang, L. Lin, Z.L. Wang, Nanoscale triboelectric-effect-enabled energy conversion for sustainably powering portable electronics, Nano Lett. 12 (2012) 6339–6346.

[56] S.M. Niu, S.H. Wang, L. Lin, Y. Liu, Y.S. Zhou, Y.F. Hu, Z.L. Wang, Theoretical study of contact-mode triboelectric nanogenerators as an effective power source, Energy Environ. Sci. 6 (2013) 3576–3583.

[57] X. Wang, Z.L. Wang, Y. Yang, Hybridized nanogenerator for simultaneously scavenging mechanical and thermal energies by electromagnetic-triboelectric-thermoelectric effects, Nano Energy 26 (2016) 164–171.

[58] Y. Yang, Z.L. Wang, Hybrid energy cells for simultaneously harvesting multi-types of energies, Nano Energy 14 (2015) 245–256.

[59] S.H. Wang, X. Wang, Z.L. Wang, Y. Yang, Efficient scavenging of solar and wind energies in a smart city, ACS Nano 10 (2016) 5696–5700.

[60] Y.C. Wu, X.D. Zhong, X. Wang, Y. Yang, Z.L. Wang, Hybrid energy cell for simultaneously harvesting wind, solar, and chemical energies, Nano Res 7 (2014) 1631–1639.

[61] X.N. Wen, Y.J. Su, Y. Yang, H.L. Zhang, Z.L. Wang, Applicability of triboelectric generator over a wide range of temperature, Nano Energy 4 (2014) 150–156.

[62] Y.C. Wu, X. Wang, Y. Yang, Z.L. Wang, Hybrid energy cell for harvesting mechanical energy from one motion using two approaches, Nano Energy 11 (2015) 162–170.

[63] T. Quan, Y.C. Wu, Y. Yang, Hybrid electromagnetic–triboelectric nanogenerator for harvesting vibration energy, Nano Res 8 (2015) 3272–3280.

[64] Q. Xu, H. Wang, Z.L. Gao, Z.H. Mao, J.P. He, M.G. Sun, A novel mat-based system for position-varying wireless power transfer to biomedical implants, IEEE Trans. Magn. 49 (2013) 4774–4779.

[65] X. Huang, Y.H. Liu, G.W. Kong, J.H. Seo, Y.J. Ma, K.I. Jang, J.A. Fan, S.M. Mao, Q. W. Chen, D.Z. Li, H. Liu, C.X. Wang, D. Patnaik, L.M. Tian, G.A. Salvatore, X. Feng, Z.Q. Ma, Y.G. Huang, J.A. Rogers, Epidermal radio frequency electronics for wireless power transfer, Microsyst. Nanoeng. 2 (2016) 16052.

[66] F. Zhang, M. Prigge, F. Beyriere, S.P. Tsunoda, J. Mattis, O. Yizhar, P. Hegemann, K. Deisseroth, Red-shifted optogenetic excitation: a tool for fast neural control derived from *Volvox carteri*, Nat. Neurosci. 11 (2008) 631–633.

[67] Z.C. He, C.M. Zhong, S.J. Su, M. Xu, H.B. Wu, Y. Cao, Enhanced power-conversion efficiency in polymer solar cells using an inverted device structure, Nat. Photon. 6 (2012) 591–595.

[68] T. Nishida, H. Saito, N. Kobayashi, Efficient and high-power AlGaN-based ultraviolet light-emitting diode grown on bulk GaN, Appl. Phys. Lett. 79 (2001) 711–712.

[69] W.L. Ng, M.A. Lourenco, R.M. Gwilliam, S. Ledain, G. Shao, K.P. Homewood, An efficient room-temperature silicon-based light-emitting diode, Nature 410 (2001) 192–194.

[70] A. Adhikari, T.N. Lerner, J. Finkelstein, S. Pak, J.H. Jennings, T.J. Davidson, E. Ferenczi, L.A. Gunaydin, J.J. Mirzabekov, L. Ye, S.Y. Kim, A. Lei, K. Deisseroth, Basomedial amygdala mediates top-down control of anxiety and fear, Nature 527 (2015) 179–185.

[71] P. Rajasethupathy, S. Sankaran, J.H. Marshel, C.K. Kim, E. Ferenczi, S.Y. Lee, A. Berndt, C. Ramakrishnan, A. Jaffe, M. Lo, C. Liston, K. Deisseroth, Projections

from neocortex mediate top-down control of memory retrieval, Nature 526 (2015) 653–659.
[72] K.L. Montgomery, A.J. Yeh, J.S. Ho, V. Tsao, S.M. Iyer, L. Grosenick, E.A. Ferenczi, Y. Tanabe, K. Deisseroth, S.L. Delp, A.S.Y. Poon, Wirelessly powered, fully internal optogenetics for brain, spinal and peripheral circuits in mice, Nat. Methods 12 (2015) 969–974.
[73] H. Wang, B. Wang, K.P. Normoyle, K. Jackson, K. Spitler, M.F. Sharrock, C. M. Miller, C. Best, D. Llano, R. Du, Brain temperature and its fundamental properties: a review for clinical neuroscientists, Front. Neurosci. 8 (2014) 307.
[74] T.I. Kim, J.G. McCall, Y.H. Jung, X. Huang, E.R. Siuda, Y.H. Li, J.Z. Song, Y. M. Song, H.A. Pao, R.H. Kim, C.F. Lu, S.D. Lee, I.S. Song, G. Shin, R. Al-Hasani, S. Kim, M.P. Tan, Y.G. Huang, F.G. Omenetto, J.A. Rogers, M.R. Bruchas, Injectable, cellular-scale optoelectronics with applications for wireless optogenetics, Science 340 (2013) 211–216.
[75] J. Mattis, K.M. Tye, E.A. Ferenczi, C. Ramakrishnan, D.J. O'Shea, R. Prakash, L. A. Gunaydin, M. Hyun, L.E. Fenno, V. Gradinaru, O. Yizhar, K. Deisseroth, Principles for applying optogenetic tools derived from direct comparative analysis of microbial opsins, Nat. Methods 9 (2012) 159–172.
[76] International Commission on Non-Ionizing Radiation Protection, Guidelines for limiting exposure to time-varying electric and magnetic fields (1 Hz to 100 kHz), Health Phys. 99 (2010) 818–836.
[77] T. Yanagisawa, T. Kojima, Degradation of InGaN blue light-emitting diodes under continuous and low-speed pulse operations, Microelectron. Reliab. 43 (2003) 977–980.
[78] H.E. Lee, J. Choi, S.H. Lee, M. Jeong, J.H. Shin, D.J. Joe, D. Kim, C.W. Kim, J. H. Park, J.H. Lee, D. Kim, C.-S. Shin, K.J. Lee, Monolithic flexible vertical GaN light-emitting diodes for a transparent wireless brain optical stimulator, Adv. Mater. 30 (2018), 1800649.
[79] K. Tajima, K. Ikeda, Y. Tanabe, E.A. Thomson, T. Yoneshiro, Y. Oguri, M.D. Ferro, A.S.Y. Poon, S. Kajimura, Wireless optogenetics protects against obesity via stimulation of non-canonical fat thermogenesis, Nat. Commun. 11 (2020) 1730.
[80] V.A. Gutzeit, K. Ahuna, T.L. Santos, A.M. Cunningham, M.S. Rooney, A.M. Zamora, C.A. Denny, Z.R. Donaldson, Optogenetic reactivation of prefrontal social neural ensembles mimics social buffering of fear, Neuropsychopharmacology 45 (2020) 1068–1077.
[81] E.S.S.J. Javaheri, M.R. Bigdeli, M.I. Zibaii, L. Dargahi, H.R. Pouretemad, Optogenetic stimulation of the anterior cingulate cortex ameliorates autistic-like behaviors in rats induced by neonatal isolation, caudate putamen as a site for alteration, NeuroMolecular Med. 21 (2019) 132–142.
[82] A. Ghaffarinejad, J.Y. Hasani, R. Hinchet, Y. Lu, H. Zhang, A. Karami, D. Galayko, S.-W. Kim, P. Basset, A conditioning circuit with exponential enhancement of output energy for triboelectric nanogenerator, Nano Energy 51 (2018) 173–184.
[83] N.C. Klapoetke, Y. Murata, S.S. Kim, S.R. Pulver, A.B. Benson, Y.K. Cho, T. K. Morimoto, A.S. Chuong, E.J. Carpenter, Z. Tian, J. Wang, Y. Xie, Z. Yan, Y. Zhang, B.Y. Chow, B. Surek, M. Melkonian, V. Jayaraman, M.C. Paton, G.K.-S. Wong, E.S. Boyden, Nat. Methods 11 (2014) 338–346.
[84] V. Sreenivasan, K. Karmakar, F.M. Rijli, C.C.H. Petersen, Parallel pathways from motor and somatosensory cortex for controlling whisker movements in mice, Eur. J. Neurosci. 41 (2015) 354–367.
[85] V. Grinevich, M. Brecht, P. Osten, Monosynaptic pathway from rat vibrissa motor cortex to facial motor neurons revealed by lentivirus-based axonal tracing, J. Neurosci. 25 (2005) 8250–8258.
[86] C.C.H. Petersen, Cortical control of whisker movement, Annu. Rev. Neurosci. 37 (2014) 183–203.
[87] K. Oda, J. Vierock, S. Oishi, S. Rodriguez-Rozada, R. Taniguchi, K. Yamashita, J. S. Wiegert, T. Nishizawa, P. Hegemann, O. Nureki, Crystal structure of the red light-activated channelrhodopsin Chrimson, Nat. Commun. 9 (2018) 3949.
[88] G. Nagel, D. Ollig, M. Fuhrmann, S. Kateriya, A.M. Mustl, E. Bamberg, P. Hegemann, Channelrhodopsin-1: a light-gated proton channel in green algae, Science 296 (2002) 2395–2398.
[89] G. Nagel, T. Szellas, W. Huhn, S. Kateriya, N. Adeishvili, P. Berthold, D. Ollig, P. Hegemann, E. Bamberg, Channelrhodopsin-2, a directly light-gated cation-selective membrane channel, Proc. Natl. Acad. Sci. U.S.A. 100 (2003) 13940–13945.
[90] R.M. Rich, D.L. Stankowska, B.P. Maliwal, T.J. Sorensen, B.W. Laursen, R. R. Krishnamoorthy, Z. Gryczynski, J. Borejdo, I. Gryczynski, R. Fudala, Elimination of autofluorescence background from fluorescence tissue images by use of time-gated detection and the AzaDiOxaTriAngulenium (ADOTA) fluorophore, Anal. Bioanal. Chem. 405 (2013) 2065–2075.
[91] J. Kapuscinski, DAPI: a DNA-specific fluorescent probe, Biotech. Histochem. 70 (1995) 220–233.
[92] L. Baldassarri, A. Gelosia, E. Fiscarelli, G. Donelli, M. Mignozzi, G. Rizzoni, Microbial colonization of implanted silicone and polyurethane catheters, J. Mater. Sci. Med. 5 (1994) 601–605.
[93] K. Ishii, E. Kodani, S. Miyamoto, T. Otsuka, M. Hosone, K.-I. Ogata, W. Sato, S. Matsumoto, T. Tadera, C. Ibuki, Y. Kusama, H. Atarashi, Pacemaker contact dermatitis: the effective use of a polytetrafluoroethylene sheet, Pacing Clin. Electrophysiol. 29 (2006) 1299–1302.
[94] G.M. Viola, J. Rosenblatt, I.I. Raad, R.O. Darouiche, Comparison of bacterial adherence to titanium versus polyurethane for cardiac implantable electronic devices, Am. J. Cardiol. 111 (2013) 1764–1766.
[95] W.L. Holman, S.V. Pamboukian, S.C. Bellot, P.S. Blood, J.A. Tallaj, J.L. Sharpton, J. K. Kirklin, Use of an intraperitoneal ventricular assist device with a polytetrafluoroethylene barrier decreases infections, J. Heart Lung Transplant. 27 (2008) 268–271.
[96] H. Yang, M. Wang, M. Deng, H. Guo, W. Zhang, H. Yang, Y. Xi, X. Li, C. Hu, Z. Wang, A full-packaged rolling triboelectric-electromagnetic hybrid nanogenerator for energy harvesting and building up self-powered wireless systems, Nano Energy 56 (2019) 300–306.

Dr. Han Eol Lee is currently working as a postdoctoral research fellow in Mechanical Engineering at Massachusetts Institute of Technology (MIT). He received his B.S., M.S., and Ph.D. degrees in Materials Science and Engineering from Korea Advanced Institute of Science (KAIST) in 2013, 2015 and 2018, respectively. His Ph.D. thesis focused on flexible micro LEDs for display and biomedical applications. His current research interests include high-performance III-V materials for wearable and skin electronics.

Prof. Jung Hwan Park is currently a professor in the Department of Mechanical Engineering at Kumoh National Institute of Technology. Prof. Park received his B.S. degree in Mechanical Engineering from Sungkyunkwan University and M.S. degree from Korea Advanced Institute of Science and Technology (KAIST), respectively. In 2018, he received his Ph.D. degree in Materials Science and Engineering from KAIST. He was previously a postdoctoral research fellow in the Department of Mechanical Engineering at University of California, Berkeley. His research interests are the novel light-material interaction technologies for wearable electronic materials and devices.

Dahee Jang received her B.S. in Biological Sciences from Ajou University in 2017. She is a Ph.D. candidate in Neuroscience from Korea Advanced Institute of Science (KAIST), under the supervision of Prof. Daesoo Kim. Her doctoral thesis is about the neural mechanisms behind action selection and initiation of innate behavior.

Prof. Daesoo Kim received a Ph.D. degree in Genetics and Neuroscience from the Pohang University of Science &Technology (POSTECH) in 1998. He performed post-doctoral research at the State University of New York(SUNY) medical school and worked at Korea Institute of Science & Technology (KIST) as senior scientist. He is currently studying about the circuit-based mechanism of motor behavior at Korea Advanced Institute of Science & Technology (KAIST). He has presented as to 'brain-inspired solutions for the crowded earth' at the World Economic Forum at Davos and won the 3.1 prize from the Samil foundation.

Prof. Keon Jae Lee received his Ph.D. in Materials Science and Engineering (MSE) at University of Illinois, Urbana-Champaign (UIUC). During his Ph.D. at UIUC, he involved in the first co-invention of "Flexible Single-crystalline Inorganic Electronics", using top-down semiconductors and soft lithographic transfer. Since 2009, he has been a professor in MSE at KAIST. His current research topics are self-powered flexible electronic systems including energy harvesting/storage devices, IoT sensor, LEDs, large scale integration (LSI), high density memory and laser material interaction for *in-vivo* biomedical and flexible application.

Dr. Geon-Tae Hwang is currently working as a senior researcher in Korea Institute of Materials Science (KIMS). He received his B.S. degree in Advanced Materials Science and Engineering from Sungkyunkwan University (SKKU) and M.S. degree from Korea Advanced Institute of Science and Technology (KAIST), respectively. His research interests are the magneto-electric conversion, energy harvesting, and magnetic sensing.